Quantum mechanical response of coupled metallic slabs

2006 J. Phys.: Condens. Matter 18 8217

(http://iopscience.iop.org/0953-8984/18/35/009)

INSTITUTE OF PHYSICS PUBLISHING JOURNAL OF PHYSICS: CONDENSED MATTER

J. Phys.: Condens. Matter **18** (2006) 8217–8228 doi:10.1088/0953-8984/18/35/009

Quantum mechanical response of coupled metallic slabs

V Despoja, L Marušić[1] and M Šunjić

Department of Physics, University of Zagreb, Bijenička 32, HR-10000 Zagreb, Croatia

E-mail: vito@phy.hr

Received 6 June 2006, in final form 21 July 2006
Published 15 August 2006
Online at stacks.iop.org/JPhysCM/18/8217

Abstract

The nonlocal dynamical polarizability of two arbitrarily shaped objects coupled by long-range Coulomb forces, when overlap of their electron densities is negligible, is calculated by expressing it in terms of the response functions of separate objects. That enables us to extend the density functional theory approach within the Kohn–Sham scheme to such systems. The method is applied to the system consisting of two metallic slabs within the jellium model. The obtained response function of the total system is used to calculate the correlation energy of a static test charge placed in the system.

1. Introduction

The dielectric response of simple systems such as semi-infinite metals, slabs or spheres within the jellium model has been extensively studied using the density functional theory (DFT) [1, 2], with a number of improvements beyond the local density approximation (LDA), e.g. using the GW approximation [3] or various forms of exchange–correlation functionals in the time-dependent local density approximation (TDLDA) method [4]. For metallic monolayers the response was also calculated in a more realistic model, using the *ab initio* methods [5]. However, much less effort has been made to study the response in a wide range of systems involving two or more objects, e.g. parallel metallic and/or dielectric slabs. The calculation of the polarizability of such systems, as well as the dynamically screened nonlocal interaction propagator which can be derived from the polarizability, can be very useful as a basis for theoretical studies of their properties, including scattering processes or effective forces between the subsystems, or in the analysis of quantum mechanical effects in the screening and excitations in heterostructures, e.g. superlattices [6–8].

While the classical dielectric theory can be easily extended to treat excitations in systems consisting of two or more objects coupled by long-range Coulomb potentials, the quantum mechanical approach to this problem presents serious difficulties. Recently a number of papers

[1] Present address: Department of Transport and Maritime Studies, University of Zadar, M Pavlinovića b.b., HR-23000 Zadar, Croatia.

attempted to treat the interaction between such systems at the level of accuracy equal to that of a single system, i.e. by treating the whole system, consisting of two parts (usually slabs), as one. The standard procedure is the following: (1) solve the appropriate Kohn–Sham equation for the whole system, (2) calculate the random-phase-approximation (RPA) density–density response function, and (3) use the so-called adiabatic-connection formula (ACF) to calculate ground state exchange–correlation energy [9]. To include short-range correlation effects beyond RPA, one can use the energy optimized exchange–correlation kernel, which (via ACF) provides accurate correlation energy in a uniform electron gas [10, 11]. Alternatively, one can implement the GW scheme to calculate interaction between two very thin metallic slabs [12].

Similar results were calculated in the extended DFT calculation for two semi-infinite solids with parallel surfaces separated at large distances [13], and for two metallic slabs separated by a shorter distance (including van der Waals saturation) [14], where again ACF was used as a starting point but the main intention was to extract the van der Waals functional from it. The method of [13, 14] is computationally more efficient but the approximations, e.g. the use of the local dielectric function, make it less accurate.

Even without getting into details of these theories, it soon becomes obvious that the standard DFT calculations encounter numerical difficulties if both slabs together with the medium between them are treated as a single system, simply because the total width of the system becomes too large for the efficient numerical treatment. Therefore the calculations are usually limited to very thin slabs (5–10 au) separated by vacuum gaps of up to 10 au. Such an approach includes full short-range correlations, leading e.g. to repulsive potentials at short distances [15], but cannot reach the van der Waals limit at large separations.

In this paper we develop an efficient method that enables us to perform exact calculations for two jellium systems coupled via Coulomb interaction, but is restricted to situations in which electron densities of the two systems do not overlap[2].

In section 2 we find a general expression for the dynamically screened response function in a system consisting of two jellium subsystems, coupled via Coulomb potentials. From the infinite summations of diagrams for the irreducible polarizabilities, or the equivalent integral equations, we obtain a set of integral equations for the total response function, containing only the response functions of the subsystems. In section 3 we apply our general theory to the system consisting of two parallel jellium slabs of arbitrary thicknesses and densities, where we can use the symmetry of the system to transform a set of integral equations into a set of matrix equations. Knowing the response function we can calculate the dynamically screened nonlocal potential $W(\mathbf{Q}, \omega, z, z')$. In section 4 we apply these results to calculate the correlation energy for a static test charge.

This derivation of the dynamically screened nonlocal potential provides a useful theoretical tool in the many-body approach to a wide range of problems, like those mentioned earlier [6–8].

2. General formalism

Our system consists of two objects of arbitrary shapes with electron charge densities $n_1(\mathbf{r})$ and $n_2(\mathbf{r})$ extending within the volumes V_1 and V_2, respectively. It is assumed that the systems are separated, i.e. that their electron charge densities do not overlap, which is the case in many physically interesting realistic situations.

In order to calculate the response function $\mathcal{R}$ of the total system, we first define the exact integral equation for the response functions R_i of each object, diagrammatically shown in

[2] An analogous idea has already been used e.g. to calculate van der Waals forces between two spherical particles within a purely classical description of their dielectric properties [16].

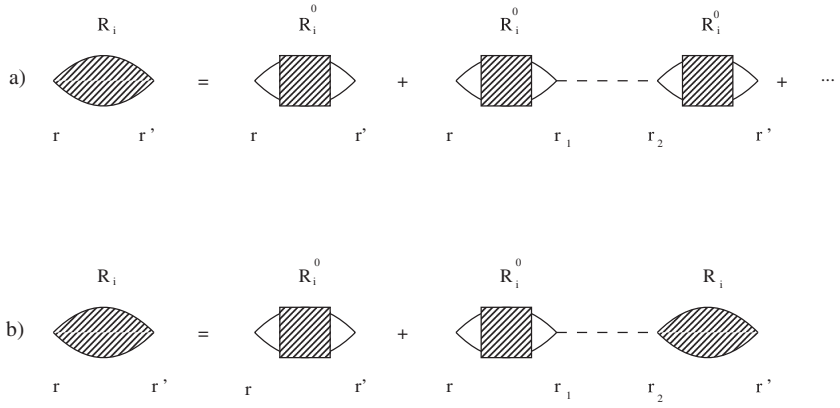

Figure 1. Feynman diagrams for the screened response function $R_i(\mathbf{r}, \mathbf{r}')$ ($\mathbf{r}, \mathbf{r}' \in V_i$, $i = 1, 2$) in a single slab: (a) infinite summation; (b) integral equation. R_i^0 is the irreducible polarizability, and the dashed line is the bare Coulomb potential.

figure 1,

$$R_i\left(\mathbf{r}, \mathbf{r}', \omega\right) = \tilde{R}_i^0\left(\mathbf{r}, \mathbf{r}', \omega\right) + \int\int \mathrm{d}^3\mathbf{r}_1\, \mathrm{d}^3\mathbf{r}_2\, \tilde{R}_i^0\left(\mathbf{r}, \mathbf{r}_1, \omega\right) v\left(\mathbf{r}_1, \mathbf{r}_2\right) R_i\left(\mathbf{r}_2, \mathbf{r}'\omega\right); \qquad i = 1, 2 \tag{1}$$

where $v(\mathbf{r}, \mathbf{r}')$ is the bare Coulomb interaction,

$$v\left(\mathbf{r}, \mathbf{r}'\right) = \frac{e^2}{|\mathbf{r} - \mathbf{r}'|} \tag{2}$$

and $\tilde{R}_i^0$ the irreducible electron polarizability. Replacing $\tilde{R}_i^0$ with the single pair excitation diagram

$$R_i^0\left(\mathbf{r}, \mathbf{r}'\omega\right) = \sum_{n,m} \frac{f_m - f_n}{\omega - E_n + E_m + \mathrm{i}\eta} \phi_n(\mathbf{r})\, \phi_m(\mathbf{r})\, \phi_n\left(\mathbf{r}'\right) \phi_m\left(\mathbf{r}'\right); \qquad i = 1, 2 \tag{3}$$

corresponds to the standard RPA. Using the free-electron wavefunctions for ϕ_n would lead to the Lindhard response function, but we shall use the Kohn–Sham wavefunctions calculated within the LDA. Thus we shall obtain the KS-LDA response function, by use of which we get beyond RPA and obtain adequate response functions of separate systems. Electrostatic Coulomb interaction and short-range exchange–correlation effects are locally included through LDA wavefunctions, while the long-range effects are included through the integral equation (1), i.e. infinite summation as in figure 1. However, possible coupling between the excitation modes of separate objects still remains to be included.

To take this coupling into account we can use the diagrammatic approach. We can distinguish four different classes of diagrams, depending on the spatial position of points $\mathbf{r}$ and $\mathbf{r}'$, leading to four integral equations:

(1) $\mathbf{r}, \mathbf{r}' \in V_1$

$$R_{11}\left(\mathbf{r}, \mathbf{r}', \omega\right) = R_1\left(\mathbf{r}, \mathbf{r}', \omega\right) + \int_{V_2} \mathrm{d}^3\mathbf{r}_1 \int_{V_1} \mathrm{d}^3\mathbf{r}_2\, \Pi_{12}\left(\mathbf{r}, \mathbf{r}_1, \omega\right) v\left(\mathbf{r}_1, \mathbf{r}_2\right) R_{11}\left(\mathbf{r}_2, \mathbf{r}'\omega\right). \tag{4}$$

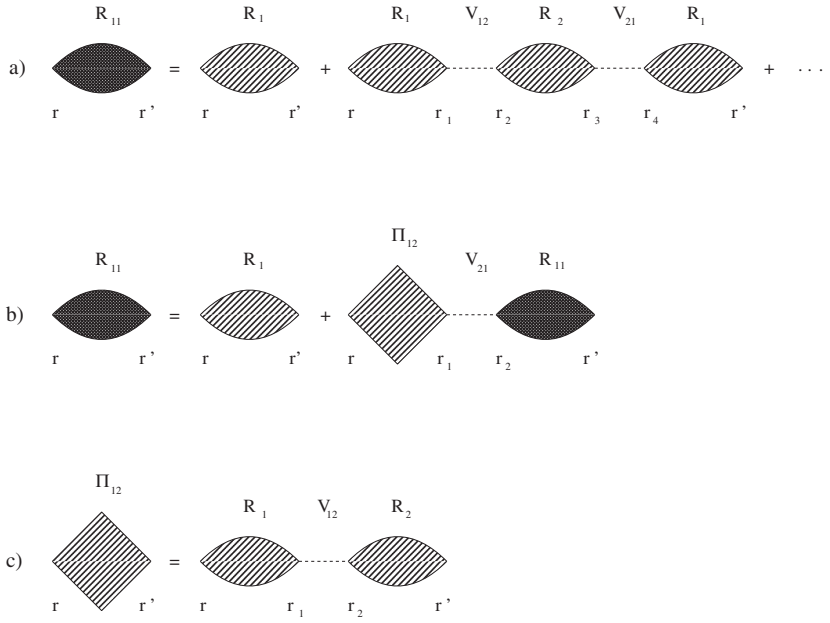

Figure 2. Feynman diagrams for the screened response function $R_{11}(\mathbf{r}, \mathbf{r}')$ in slab 1 ($\mathbf{r}$, $\mathbf{r}_1$, $\mathbf{r}_4$, $\mathbf{r}' \in V_1$) coupled to slab 2 ($\mathbf{r}_2$, $\mathbf{r}_3 \in V_2$). (a) Infinite summation; (b) integral equation; (c) diagrammatic representation of $\Pi_{12}(\mathbf{r}, \mathbf{r}')$.

Figure 2(b) represents diagrammatically this integral equation, equivalent to the infinite summation of diagrams (figure 2(a)).

(2) $\mathbf{r} \in V_1$ and $\mathbf{r}' \in V_2$

$$R_{12}\left(\mathbf{r}, \mathbf{r}', \omega\right) = \Pi_{12}\left(\mathbf{r}, \mathbf{r}', \omega\right) + \int_{V_2} \mathrm{d}^3\mathbf{r}_1 \int_{V_1} \mathrm{d}^3\mathbf{r}_2\, \Pi_{12}\left(\mathbf{r}, \mathbf{r}_1, \omega\right) v\left(\mathbf{r}_1, \mathbf{r}_2\right) R_{12}\left(\mathbf{r}_2, \mathbf{r}'\omega\right). \tag{5}$$

This integral equation is represented in figure 3(b), with the corresponding infinite series of diagrams in figure 3(a).

(3) $\mathbf{r} \in V_2$ and $\mathbf{r}' \in V_1$

$$R_{21}\left(\mathbf{r}, \mathbf{r}', \omega\right) = \Pi_{21}\left(\mathbf{r}, \mathbf{r}', \omega\right) + \int_{V_1} \mathrm{d}^3\mathbf{r}_1 \int_{V_2} \mathrm{d}^3\mathbf{r}_2\, \Pi_{21}\left(\mathbf{r}, \mathbf{r}_1, \omega\right) v\left(\mathbf{r}_1, \mathbf{r}_2\right) R_{21}\left(\mathbf{r}_2, \mathbf{r}'\omega\right). \tag{6}$$

This case is also illustrated in figure 3, after replacing the volume V_1 by V_2.

(4) $\mathbf{r}, \mathbf{r}' \in V_2$

Again, after replacing V_1 by V_2 the next integral equation is shown in figure 2.

$$R_{22}\left(\mathbf{r}, \mathbf{r}', \omega\right) = R_2\left(\mathbf{r}, \mathbf{r}', \omega\right) + \int_{V_1} \mathrm{d}^3\mathbf{r}_1 \int_{V_2} \mathrm{d}^3\mathbf{r}_2\, \Pi_{21}\left(\mathbf{r}, \mathbf{r}_1, \omega\right) v\left(\mathbf{r}_1, \mathbf{r}_2\right) R_{22}\left(\mathbf{r}_2, \mathbf{r}'\omega\right) \tag{7}$$

where

$$\Pi_{12}\left(\mathbf{r}, \mathbf{r}', \omega\right) = \int_{V_1} \mathrm{d}^3\mathbf{r}_1 \int_{V_2} \mathrm{d}^3\mathbf{r}_2\, R_1\left(\mathbf{r}, \mathbf{r}_1, \omega\right) v\left(\mathbf{r}_1, \mathbf{r}_2\right) R_2\left(\mathbf{r}_2, \mathbf{r}'\omega\right) \tag{8}$$

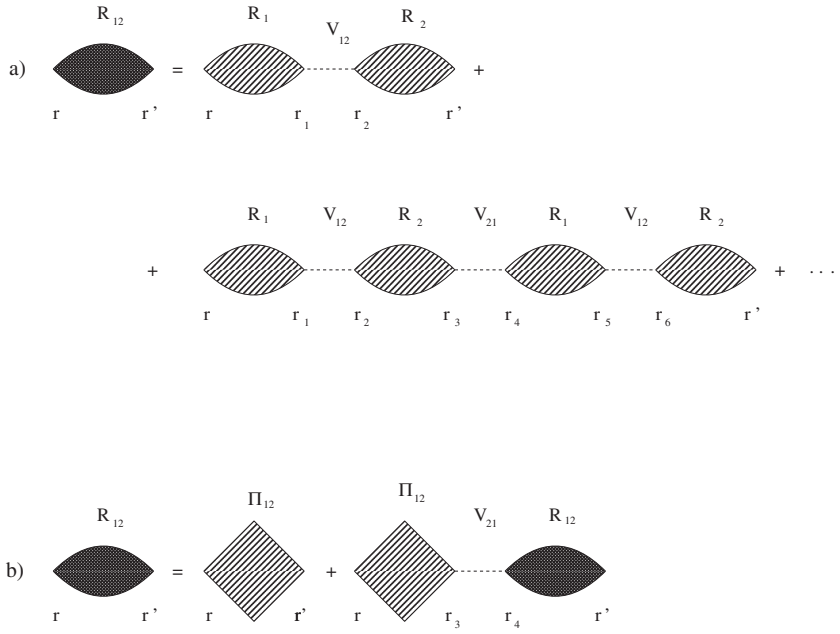

Figure 3. Feynman diagrams for the screened response function $R_{12}(\mathbf{r}, \mathbf{r}')$ connecting slabs 1 and 2 ($\mathbf{r}, \mathbf{r}_1, \mathbf{r}_4, \mathbf{r}_5 \in V_1$, $\mathbf{r}_2, \mathbf{r}_3, \mathbf{r}_6, \mathbf{r}' \in V_2$). (a) Infinite summation; (b) integral equation.

and

$$\Pi_{21}\left(\mathbf{r}, \mathbf{r}', \omega\right) = \int_{V_2} \mathrm{d}^3\mathbf{r}_1 \int_{V_1} \mathrm{d}^3\mathbf{r}_2 \, R_2\left(\mathbf{r}, \mathbf{r}_1, \omega\right) v\left(\mathbf{r}_1, \mathbf{r}_2\right) R_1\left(\mathbf{r}_2, \mathbf{r}'\omega\right) \tag{9}$$

represent Coulomb coupling between charge fluctuation in different objects (figure 3(c)).

After solving equations (4)–(7) and obtaining functions R_{11}, R_{12}, R_{21} and R_{22}, the response function $\mathcal{R}$ of the total system is calculated as

$$\mathcal{R}\left(\mathbf{r}, \mathbf{r}'\omega\right) = \sum_{i=1,2} \sum_{j=1,2} R_{ij}\left(\mathbf{r}, \mathbf{r}'\omega\right). \tag{10}$$

This general procedure can be applied to any system consisting of two objects with non-overlapping electron densities, but we shall specify the results for the planar geometry and calculate the response function of two metallic (jellium) slabs.

3. Application to two metallic slabs

We assume one of the slabs in the region $-L_1 \leqslant z \leqslant 0$ with electron density corresponding to r_{s1}, and the other one in the region $d \leqslant z \leqslant d + L_2$ with electron density corresponding to r_{s2}. In other words, d is the distance between the points where the electron densities of the two slabs practically vanish, while the distance between jellium edges is $D = d + 2\Delta$ (figure 4), where Δ is the characteristic electron density decay length. The jellium thicknesses are then $a_1 = L_1 - 2\Delta$ and $a_2 = L_2 - 2\Delta$. The regions of special interest to us are the regions where electron density is equal to zero, and we shall denote them by L ($z < -L_1$, i.e. left from the

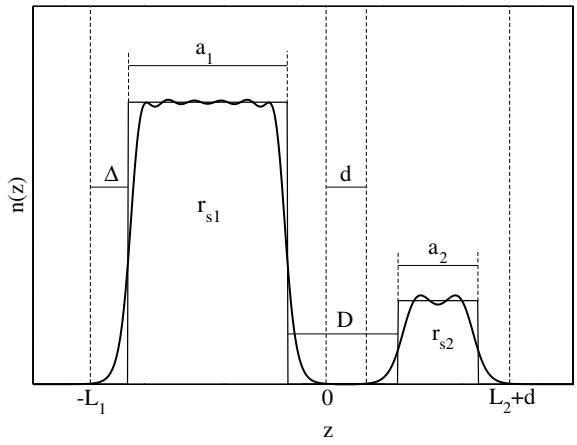

Figure 4. Electron density for two metallic slabs. D is the separation between the jellium edges, while electron charge densities of the slabs are separated by $d = D - 2\Delta$.

left slab), R ($z > L_2$, i.e. right from the right slab) and I ($0 < z < d$, i.e. the intermediate region).

Due to the planar symmetry of the system, all quantities could be Fourier transformed in the $\boldsymbol{\rho}$ direction as

$$f(\mathbf{Q}, z, z') = \int_A \mathrm{d}\boldsymbol{\rho}\, \mathrm{e}^{\mathrm{i}\mathbf{Q}\boldsymbol{\rho}} f(\mathbf{r}, \mathbf{r}') \tag{11}$$

$$f(\mathbf{r}, \mathbf{r}') = \frac{1}{(2\pi)^2} \int \mathrm{d}\mathbf{Q}\, \mathrm{e}^{-\mathrm{i}\mathbf{Q}\boldsymbol{\rho}} f(\mathbf{Q}, z, z') \tag{12}$$

where A is the surface of the metal and $\mathbf{Q}$ is the component of the wavevector parallel to the surface.

For clarity, from now on, we shall omit the variables (conserved quantities) ω and $\mathbf{Q}$ as arguments of the functions R and Π. Equations (1) transform into

$$R_i\left(z, z'\right) = R_i^0\left(z, z'\right) + \int_{-\infty}^{\infty} \int_{-\infty}^{\infty} \mathrm{d}z_1\, \mathrm{d}z_2 R_i^0\left(z, z_1\right) V\left(z_1, z_2\right) R_i\left(z_2, z'\right) \tag{13}$$

where $i = 1, 2$. KS-LDA response functions can now be written in the form [17, 18]

$$R_i^0\left(z, z'\right) = \sum_{n=1}^{n_M} \sum_{m=1}^{\infty} F_{n,m}\left(Q, \omega\right) \phi_n\left(z\right) \phi_m\left(z\right) \phi_n\left(z'\right) \phi_m\left(z'\right); \qquad i = 1, 2 \tag{14}$$

where the function $F(Q, \omega)$ can be calculated analytically [18, 20], and the functions ϕ are real. n_M is the number of occupied states.

The bare Coulomb interaction (2) transforms into

$$v\left(z, z'\right) = v_Q \mathrm{e}^{-Q\left|z - z'\right|}, \qquad v_Q = \frac{2\pi e^2}{Q} \tag{15}$$

and equations (4)–(7) become

$$R_{11}\left(z, z'\right) = R_1\left(z, z'\right) + \int_d^{d+L_2} \mathrm{d}z_1 \int_{-L_1}^{0} \mathrm{d}z_2\, \Pi_{12}\left(z, z_1\right) v_{21}\left(z_1, z_2\right) R_{11}\left(z_2, z'\right) \tag{16}$$

$$R_{12}\left(z, z'\right) = \Pi_{12}\left(z, z'\right) + \int_d^{d+L_2} \mathrm{d}z_1 \int_{-L_1}^{0} \mathrm{d}z_2\, \Pi_{12}\left(z, z_1\right) v_{21}\left(z_1, z_2\right) R_{12}\left(z_2, z'\right), \tag{17}$$

$$R_{21}\left(z,z'\right)=\Pi_{21}\left(z,z'\right)+\int_{-L_1}^{0}\mathrm{d}z_1\int_{d}^{d+L_2}\mathrm{d}z_2\,\Pi_{21}\left(z,z_1\right)v_{12}\left(z_1,z_2\right)R_{21}\left(z_2,z'\right) \tag{18}$$

$$R_{22}\left(z,z'\right)=R_2\left(z,z'\right)+\int_{-L_1}^{0}\mathrm{d}z_1\int_{d}^{d+L_2}\mathrm{d}z_2\,\Pi_{21}\left(z,z_1\right)v_{12}\left(z_1,z_2\right)R_{22}\left(z_2,z'\right) \tag{19}$$

with

$$\Pi_{12}\left(z,z'\right)=\int_{-L_1}^{0}\mathrm{d}z_1\int_{d}^{d+L_2}\mathrm{d}z_2\,R_1\left(z,z_1\right)v_{12}\left(z_1,z_2\right)R_2\left(z_2,z'\right) \tag{20}$$

$$\Pi_{21}\left(z,z'\right)=\int_{d}^{d+L_2}\mathrm{d}z_1\int_{-L_1}^{0}\mathrm{d}z_2\,R_2\left(z,z_1\right)v_{21}\left(z_1,z_2\right)R_1\left(z_2,z'\right) \tag{21}$$

and the function v_{12} represents the inter-slab bare Coulomb interaction:

$$v_{12}\left(z,z'\right)=v_{21}\left(z',z\right)=v_Q\mathrm{e}^{-Q\left(z'-z\right)};\qquad -L_1<z<0,\quad d<z'<d+L_2. \tag{22}$$

Indices ij; $i,j=1,2$ denote the regions in which the variables z,z' are defined, i or $j=1$ meaning the first (left) slab and i or $j=2$ meaning the second (right) slab.

To solve the integral equations (16)–(19) selfconsistently it is convenient (and much more numerically efficient) to transform them into the matrix form. Since the symmetry in the direction perpendicular to the surfaces is broken, if we perform Fourier transformation in the z direction, the integral equation does not transform into an algebraic one, but rather into a matrix equation. Functions used for this transformation should be constructed as products of the functions $u_i(z)$ and $v_i(z')$ (depending on the region of definition of variables z and z'), where each set of functions (u and v) is defined within one of the slabs.

An obvious choice is the cosine functions (commonly used for a single slab [18, 19]) defined as

$$\begin{array}{ll}
-L_1<z<0 & d<z'<d+L_2\\
u_{q_1}(z)=\dfrac{2}{L_1}\eta_{q_1}\cos(q_1z) & v_{q_2}\left(z'\right)=\dfrac{2}{L_2}\eta_{q_2}\cos\left[q_2\left(z'-d\right)\right]\\
\eta_{q_1}=1-\frac{1}{2}\delta_{q_1,0} & \eta_{q_2}=1-\frac{1}{2}\delta_{q_2,0}\\
q_1=\dfrac{n\pi}{L_1}; & q_2=\dfrac{n\pi}{L_2}
\end{array} \tag{23}$$

where $n=0,1,2,3,\ldots$ and δ is the Kronecker symbol.

For example, if z is defined in the region $-L_1<z<0$ and z' in the region $d<z'<d+L_2$, the function $f(z,z')$ can be expanded as

$$f\left(z,z'\right)=\frac{4}{L_1L_2}\sum_{q_1q_2}\eta_{q_1}\eta_{q_2}f_{q_1q_2}\cos\left(q_1z\right)\cos\left[q_2\left(z'-d\right)\right] \tag{24}$$

with

$$f_{q_1q_2}=\int_{-L_1}^{0}\mathrm{d}z\int_{d}^{d+L_2}\mathrm{d}z'\,\cos\left(q_1z\right)f\left(z,z'\right)\cos\left[q_2\left(z'-d\right)\right]. \tag{25}$$

Using (23) equations (16)–(21) become the following matrix equations:

$$R_{11}=R_1+\Pi_{12}v_{12}^{\mathrm{T}}R_{11} \tag{26}$$

$$R_{12}=\Pi_{12}+\Pi_{12}v_{12}^{\mathrm{T}}R_{12} \tag{27}$$

$$R_{21}=\Pi_{12}^{\mathrm{T}}+\Pi_{12}^{\mathrm{T}}v_{12}R_{21} \tag{28}$$

$$R_{22}=R_2+\Pi_{12}^{\mathrm{T}}v_{12}R_{22} \tag{29}$$

$$\Pi_{12}=R_1v_{12}R_2. \tag{30}$$

From equation (22) and definition (25) it is obvious that the $v_{12q_1q_2}$ Fourier component of the function $v_{12}(z, z')$ is equal to the Fourier component $v_{21q_2q_1}$ of the function $v_{21}(z, z')$, so in the equations above we were able to use the symmetry properties of the matrix v_{21},

$$v_{21} = v_{12}^{\mathrm{T}} \tag{31}$$

and also the symmetry properties of the matrices R_1 and R_2, which leads to

$$\Pi_{12}^{\mathrm{T}} = \{R_1 v_{12} R_2\}^{\mathrm{T}} = R_2^{\mathrm{T}} v_{12}^{\mathrm{T}} R_1^{\mathrm{T}} = R_2 v_{21} R_1 = \Pi_{21}. \tag{32}$$

Of course, in the symmetrical case (e.g. two slabs of equal thicknesses and electron densities) $\Pi_{12} = \Pi_{21}$ and $v_{12} = v_{21}$.

After matrix inversions of (26)–(29) we get matrices R_{11}, R_{12}, R_{21} and R_{22}, and then, after using the Fourier transformation (24), we obtain the response function of the whole system consisting of two interacting metallic slabs in z-space:

$$\mathcal{R}\left(z, z'\right) = \sum_{i,j=1,2} R_{ij}\left(z, z'\right). \tag{33}$$

It is important to note that the only input we need in order to calculate $\mathcal{R}$ is the matrices R_1^0 and R_2^0, together with the matrices v_1, v_2 and v_{12} that can be calculated analytically and are given by

$$v_{i,q_iq_i'} = \frac{2\pi e^2}{q_i^2 + Q^2}\left\{\frac{L_i}{\eta_{q_i}}\delta_{q_iq_i'} + \frac{Q}{q_i'^2 + Q^2}\left[\left(p_{q_i} + p_{q_i'}\right)\mathrm{e}^{-QL_i} - \left(1 + p_{q_i}p_{q_i'}\right)\right]\right\}; \quad i = 1, 2 \tag{34}$$

and

$$v_{12,q_1q_2} = \frac{8\pi e^2 Q}{L_1 L_2}\eta_{q_1}\eta_{q_2}\frac{\left(1 - p_{q_1}\mathrm{e}^{-QL_1}\right)\left(1 - p_{q_2}\mathrm{e}^{-QL_2}\right)}{\left(q_1^2 + Q^2\right)\left(q_2^2 + Q^2\right)}\mathrm{e}^{-Qd} \tag{35}$$

where p_{q_i} is the parity of the q_ith cosine harmonic, i.e. $p_{q_i} = (-)^{q_i L_i/2\pi}$.

All the matrices are, of course, infinite, and have to be truncated. Fortunately, due to the fast convergence, for slabs thinner than 100 a_0 the dimension never needs to be greater than 50. E.g. in our calculations we can use only 30 simple cosine harmonics.

4. Results and discussion

We can use the response function obtained in the previous section to calculate correlation energy $V_{\mathrm{c}}(z)$ for a test point charge (e.g. electron) placed inside our system. Outside the slabs this corresponds to the local (image) potential $V_{\mathrm{im}}(z)$. It is given as the energy difference between the free charge and the charge interacting with the system, and can be calculated as the real part of the localized electron self-energy for $\omega = 0$:

$$V_{\mathrm{c}}(z) = \Delta E(z) = \mathrm{Re}\,\Sigma(\omega = 0, z) = -\frac{1}{2}\int \frac{\mathrm{d}\mathbf{Q}}{(2\pi)^2}\,\mathrm{Re}\,W_{\mathrm{ind}}(\mathbf{Q}, \omega = 0, z, z) \tag{36}$$

where W_{ind} is the induced non-local screened interaction between the points z and z', and it can be related to the response function as [18]

$$W_{\mathrm{ind}}(\mathbf{Q}, \omega, z, z') = \int_{-\infty}^{\infty}\mathrm{d}z_1\int_{-\infty}^{\infty}\mathrm{d}z_2\, v\left(\mathbf{Q}, z, z_1\right)\mathcal{R}\left(\mathbf{Q}, \omega, z_1, z_2\right) v\left(\mathbf{Q}, z_2, z'\right) \tag{37}$$

where v is again given by (15). This definition of the correlation energy is equivalent to the one in [21] and represents the generalization of the classical image potential.

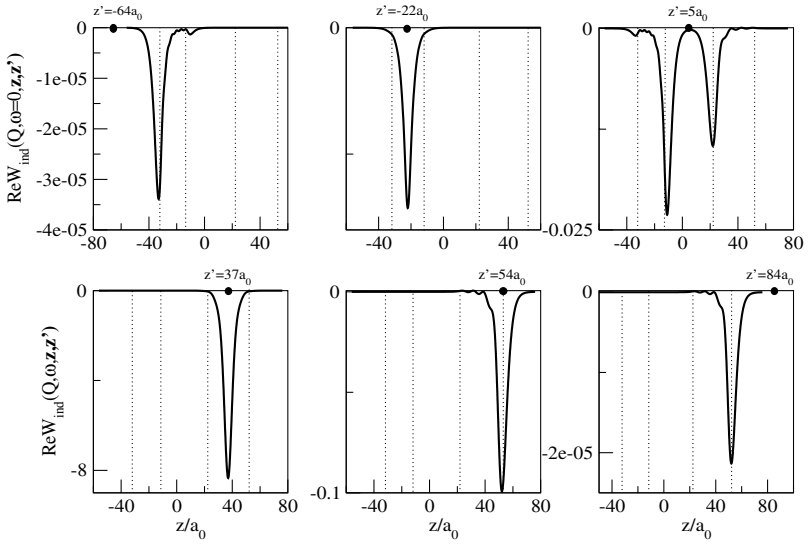

Figure 5. Propagator of the induced non-local screened interaction $W_{\rm ind}(Q, \omega = 0, z, z')$ as a function of the test charge position z' (represented by the dot), for $Q = 0.4k_{\rm F}$, $\omega = 10^{-5}E_{\rm F}$, $D = 34\ a_0$, $r_{s1} = 2$, $r_{s2} = 4$, $a_1 = 20\ a_0$ and $a_2 = 30\ a_0$. Dotted lines represent the jellium edges.

Since we used KS-LDA wavefunctions to calculate the response function, the potential $V_{\rm c}(z)$ obtained in this way is somewhat similar to the LDA exchange–correlation potential $V_{\rm XC}$. However, $V_{\rm XC}$ takes properly into account the exchange and short range correlations, which makes it more accurate than our $V_{\rm c}(z)$ for an electron inside the slab. On the other hand, since the LDA $V_{\rm XC}$ is exact for a homogeneous system and fails to include the long range correlations, it is inaccurate for an electron outside the slab. In our correlation energy $V_{\rm c}(z)$ the exchange and short-range correlations are included only through the KS-LDA wavefunctions used to calculate the response function, and not through the potential formalism, making the result inaccurate inside a slab. However, it includes the long-range correlations within RPA, which makes it more accurate outside a slab, where KS-LDA fails. For very large distances from the slab it is practically equal to the classical image potential.

We first show how the propagator of the induced non-local screened interaction $W_{\rm ind}\ (Q, \omega = 0, z, z')$ behaves for various positions of the test charge (figure 5). The test charge is placed at point z' (represented by the dot) and $W_{\rm ind}$ is then plotted as a function of z. As already shown using the non-local self-energy instead of the interaction propagator [22], the response is quite localized when the test charge is inside one of the slabs, but it becomes strongly delocalized when the test charge is outside the slabs or between them.

Figure 6 shows our quantum mechanical correlation energy $V_{\rm c}(z)$ given by (36) compared with the classical (image) potential $V_{\rm im}(z)$, calculated by solving the appropriate Poisson equation, where the boundaries of the dielectric medium are taken to be at the jellium edges. The classical potential, of course, does not depend on the electron density, while quantum mechanical effects are stronger for higher densities (small r_s). Also, if we observe the potential barrier between the slabs, it is obvious that the barrier height in the centre of the gap is not much lower than the classical one, but the difference becomes more significant as the electron moves away from the centre. In other words, the barrier width is reduced, which would have strong influence on the transmission probability for an electron moving from one slab to another with energy slightly below the barrier top.

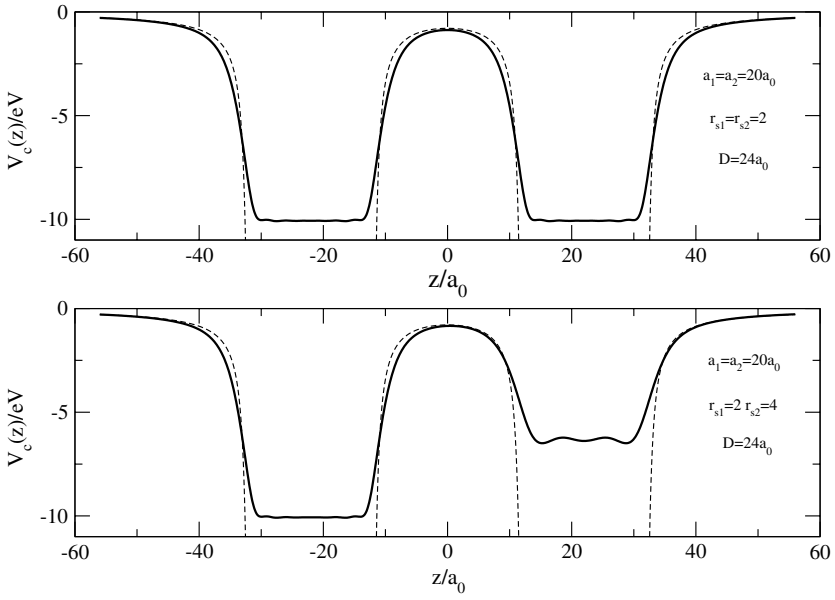

Figure 6. Correlation energy $V_c(z)$ (full line) and classical (image) potential $V_{im}(z)$ (dashed line) for the system consisting of two jellium slabs of equal thicknesses (20 au) and (a) equal electron densities, (b) different electron densities.

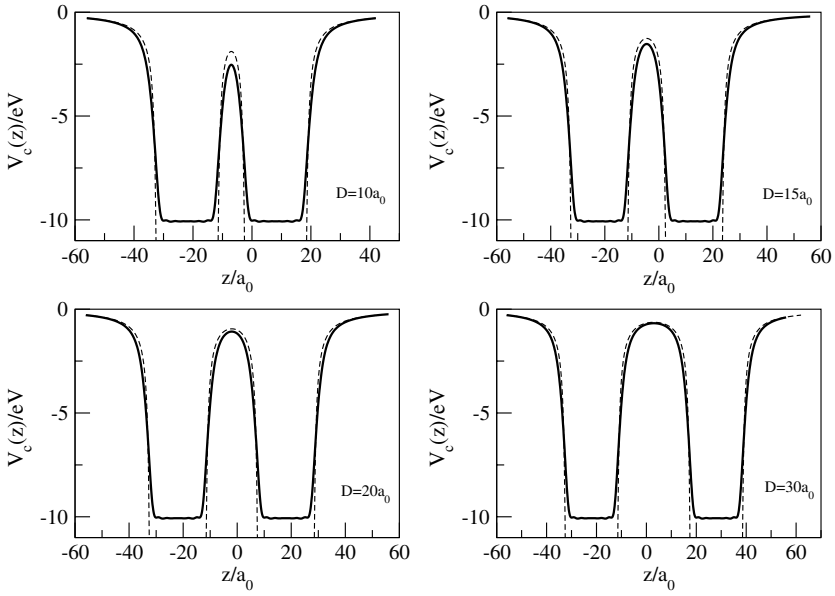

Figure 7. Correlation energy $V_c(z)$ (full line) and classical (image) potential $V_{im}(z)$ (dashed line) for the system consisting of two jellium slabs of equal thicknesses and electron densities, for four various distances between the slabs.

We also examined the influence of the slab thicknesses on the effective potential, and especially the barrier between the slabs. The classical potential does not depend on the slab

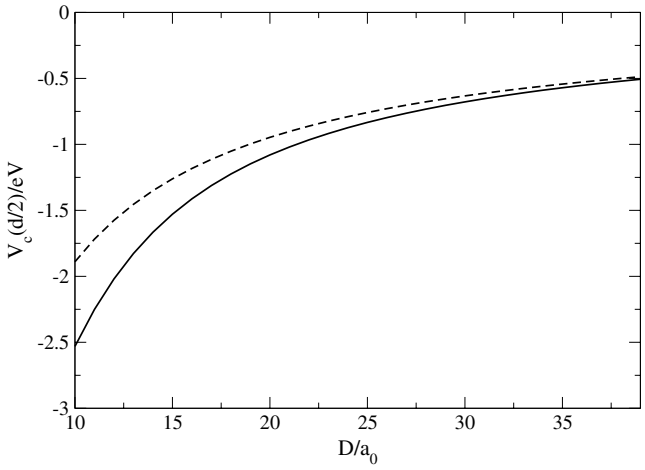

Figure 8. Barrier height as a function of the distance between slabs. The full line represents the height of the quantum mechanical correlation energy $V_c(d/2)$, while the dashed line is the height of the classical (image) potential $V_{im}(d/2)$.

thickness, but neither does the quantum mechanical one (i.e. the dependence is practically negligible). On the other hand, they both depend on the distance between the slabs, and that is shown in figure 7. Obviously, the quantum mechanical effects are much stronger for narrow gaps, i.e. when the slab surfaces are closer and the coupling of the electron to the surface excitations with larger wavevectors is stronger.

Finally, in figure 8, we show the quantum mechanical and classical barrier heights, i.e. the distance between the vacuum level and the barrier top, as functions of the distance between the slabs. As we can see, not only is the reduction of the barrier stronger for narrow gaps, but the difference between the quantum mechanical and classical results becomes more obvious. On the other hand, for gaps larger then 30 au, this difference becomes negligible.

5. Conclusion

We have presented a derivation of the polarizability of a system consisting of two separate objects interacting through Coulomb forces, in the case when the distance between the objects is large enough that their electron densities do not overlap. We applied this method to perform an efficient full LDA-KS calculation of the response of systems consisting of two different metallic (jellium) slabs, reducing the problem to the much easier single-slab calculations. The results were illustrated by the detailed discussion of the correlation energy for the static test charge. Our method can be extended to the calculation of response functions and dynamical screening propagators of more complex planar systems, like superlattices or heterostructures, and also to the study of van der Waals interaction between metallic slabs of arbitrary thicknesses and densities.

References

[1] Eguiluz A G 1983 *Phys. Rev. Lett.* **51** 1907
[2] For an extensive list of references on the jellium model of simple metal clusters see Brack M 1993 *Rev. Mod. Phys.* **65** 677

[3] Eguiluz A G, Heinrichsmeier M, Fleszar A and Hanke W 1992 *Phys. Rev. Lett.* **68** 1359
[4] Schaich W L and Dobson J F 1994 *Phys. Rev.* B **49** 14700
[5] Bergara A, Silkin V M, Chulkov E V and Echenique P M 2003 *Phys. Rev.* B **67** 245402
[6] Jain J K and Allen P B 1985 *Phys. Rev. Lett.* **54** 947
[7] Giraldo J *et al* 1988 *Phys. Rev.* B **38** 5380
[8] Vazquez-Nava R A, Cocoletzi G H, del Castillo-Mussot M and Mochan W L 1998 *Phys. Rev.* B **57** 14642
[9] Dobson J F and Wang J 1998 *Phys. Rev. Lett.* **82** 2123
[10] Dobson J F and Wang J 2000 *Phys. Rev.* B **62** 10038
[11] Jung J, Garcia Gonzalez P, Dobson J F and Godby R W 2004 *Phys. Rev.* B **70** 205107
[12] Garcia-Gonzalez P and Godby R W 2002 *Phys. Rev. Lett.* **88** 056406
[13] Andersson Y, Hult E, Appel P, Langreth D C and Lundqvist B I 1998 *Solid State Commun.* **106** 235
[14] Rydberg H, Lundqvist B I, Langreth D C and Dion M 2000 *Phys. Rev.* B **62** 6997
[15] Dobson J F and Wang J 2004 *Phys. Rev.* B **69** 235104
[16] Brako R, Šunjić M and Šips V 1974 *Solid State Commun.* **19** 161
[17] Eguiluz A G 1985 *Phys. Rev.* B **31** 3303
[18] Marušić L and Šunjić M 2001 *Phys. Scr.* **63** 336
[19] Pitarke J M and Eguiluz A G 2001 *Phys. Rev.* B **63** 045116
[20] Newns D M 1970 *Phys. Rev.* B **1** 3304
[21] Eguiluz A G, Campbell D A, Maradudin A A and Wallis R F 1984 *Phys. Rev.* B **30** 5449
[22] Deisz J J, Eguiluz A G and Hanke W 1993 *Phys. Rev. Lett.* **71** 2793